Optical near-field mapping of bright and dark quantum dot states [1]

Ulrich Hohenester [2]

Institut für Physik, Karl–Franzens–Universität Graz, Universitätsplatz 5, 8010 Graz

Abstract

We theoretically investigate scanning nearfield optical microscopy (SNOM) of semiconductor quantum dots. A general theoretical framework is developed that accounts for photo excitation and relaxation in complex dielectric environments. We find that in the nearfield regime bright and dark excitonic states become mixed, opening new channels for the coupling to the electromagnetic field.

Key words: quantum dots, scanning nearfield optical microscopy (SNOM), open system
PACS: 73.21.La, 78.67.-n, 71.35.-y

1. Introduction

Optics is a unique tool that allows a remote imaging of objects. For nano systems, with dimensions L ranging from a few to several tens of nanometers, problems arise because of the micrometer wavelength λ of light that limits the resolution of conventianal optics to $\lambda/2 \gg L$. Let us look more closely at the reasons for this limitation. We consider a quasi two-dimensional nanostructure located in the xy-plane that radiates at frequency ω. The electric component of the field at position z away from the nanostructure will be given by some Fourier transform [1]

$$\boldsymbol{E}(\boldsymbol{r},t) = \sum_{\sigma,k_x,k_y} \boldsymbol{E}_\sigma(k_x,k_y) \exp i(k_x x + k_y y + k_z z - \omega t)\,, \tag{1}$$

with σ the light polarization. Maxwell's equations tells us that for light propagating away from the nanostructure the relation

$$k_z = \sqrt{k^2 - k_x^2 - k_y^2}\,, \quad k^2 > k_x^2 + k_y^2 \tag{2}$$

must be fulfilled, where $k = \omega c^{-1}$ is the light wavevector. Because of this inequality a propagating light wave can never carry a spatial resolution greater than

$$\Delta \approx \frac{2\pi}{k_{\max}} = \frac{2\pi c}{\omega} = \lambda\,, \tag{3}$$

which is reminiscent of the Abbe limit. However, something is missing. For larger values of the transverse wave vector we get

$$k_z = i\sqrt{k_x^2 + k_y^2 - k^2}\,, \quad k^2 < k_x^2 + k_y^2\,. \tag{4}$$

These evanescent waves, which provide information about the fine spatial details of the nanostructure, decay exponentially with z. The measurement of such waves is the objective of scanning nearfield optical microscopy (SNOM) [2,3]. Conveniently, this is achieved by exciting the nanostructure through the tip of an

[1] Dedicated to the memory of Robert Heitz, in remembrance to his scientific and social contributions to the Mauterndorf winterschools.

[2] Corresponding author. E-mail: ulrich.hohenester@uni-graz.at

optical fiber (illumination mode) or collecting luminescence of the nanostructure through the tip (collection mode). Near-field spectroscopy has been successfully used for the measurement of single and coupled semiconductor nanostructures [4–6], molecules [7,8], or metallic nanostructures [9,10].

If the spatial near-field resolution falls below the extension of confined quantum systems, it becomes possible to directly map out the spatial probability distribution of the wavefunction. This was recently achieved by Matsuda et al. [11] for quantum dots where the quantum confinement is induced by local monolayer fluctuations in the thickness of a semiconductor quantum well. With $\Psi_x(\boldsymbol{r}_e, \boldsymbol{r}_h)$ the electron-hole wavefunction of the quantum dot, the matrix elements for the optical nearfield transitions are of the form [12–14]

$$\int d\boldsymbol{r}\, \boldsymbol{E}_\omega(\boldsymbol{r}_{\rm tip} - \boldsymbol{r})\Psi_x(\boldsymbol{r}, \boldsymbol{r})\,, \qquad (5)$$

with $\boldsymbol{E}_\omega(\boldsymbol{r}_{\rm tip} - \boldsymbol{r})$ the electromagnetic distribution around the nearfield tip. In contrast to the far-field, where the matrix elements governing the light-matter coupling are determined by the quantum states alone, in the near-field the pertinent matrix elements (5) become a convolution of the quantum states with the electro-magnetic field profile of the SNOM tip. This allows to break in the near-field the usual optical selection rules, and to excite dark states whose excitation is forbidden by symmetry in the far-field.

In this paper we theoretically investigate the spectral response of a semiconductor quantum dot excited in the optical near-field. We find that in order to observe dark states directly by means of optical spectroscopy it not only suffices to excite these states, e.g. by means of symmetry breaking in the near-field, but additionally new decay channels have to be opened that allow coupling to propagating photon modes.

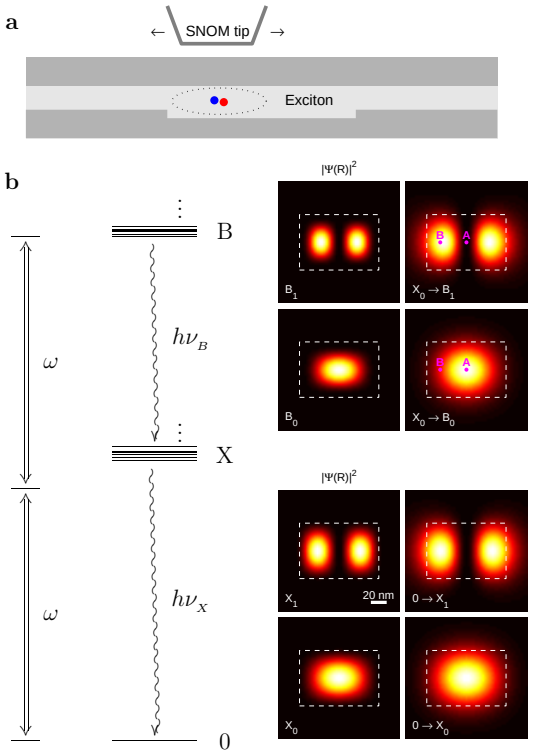

Fig. 1. (a) Schematic sketch of the confinement potential for excitons and biexcitons, which is induced by local monolayer fluctuations in the thickness of a semiconductor quantum well, and the probing SNOM tip. (b) Photoexcitation scenario assumed in our calculations. A biexciton state is excited by SNOM within a two-photon process. Because of the biexciton binding $\delta E_b \sim 4$ meV the luminescence of the biexciton-to-exciton transition is red-, and the exciton-to–groundstate transition blue-shifted with respect to ω. The insets report the square modulus of the center-of-mass part of the exciton and biexciton wave functions [14,15] (left columns) and the spatial near-field maps (right columns) for a terrace of dimension 100×70 nm (dashed line) and for a Bethe-Bouwkamp near-field probe with a full-width of half maximum of approximately 25 nm. In the optical far-field only X_0 and B_0 are allowed, whereas X_1 and B_1 are forbidden because of symmetry.

2. Theory

A proper theoretical treatment of optical nearfield microscopy of nanostructures should account on the same footing for the carrier states, the excitation of the nearfield probe, the optical decay of the carrier states in presence of a possibly modified dielectric environment, and for other environment couplings. All this constitutes a formidable theoretical challenge. Let us start with the carrier states. We consider quantum confined states induced by monolayer fluctuations in the thickness of a GaAs/AlGaAs semiconductor quantum well, fig. 1(a) [11,14]. Since the confinement length (several tens of nm) is much larger than both the lattice constant and the excitonic Bohr radius, we adopt the usual envelope function and rigid-exciton (rigid-biexciton) approximations, the latter assum-

ing that the correlated electron-hole wavefunctions factorize into a center-of-mass and a relative part given by that of the quantum well [16]. The resulting two-dimensional Schrödinger equation for the exciton and biexciton center-of-mass wavefunctions are then solved numerically [14,15]. We describe the light-matter coupling within the usual dipole and rotating wave approximations [15]

$$H_{\rm op}(t) = \int d\boldsymbol{r}\, \left(\boldsymbol{P}(\boldsymbol{r}) \boldsymbol{E}^-(\boldsymbol{r},t) + \boldsymbol{P}^\dagger(\boldsymbol{r}) \boldsymbol{E}^+(\boldsymbol{r},t) \right) . \tag{6}$$

Here, $\boldsymbol{P}(\boldsymbol{r}) = \boldsymbol{\mu}\, \Psi_h(\boldsymbol{r}) \Psi_e(\boldsymbol{r})$ is the interband polarization operator accounting for the destruction of an electron-hole pair at position $\boldsymbol{r}$, $\boldsymbol{\mu}$ is the dipole moment of the bulk semiconductor, and $\boldsymbol{E}^\pm$ are the electric field components propagating with positive or negative frequency components. For simplicity, we shall not indicate explicitly the spin and polarization degrees of freedom. Equation (6) holds for both classical and quantum light fields, where in the former case $\boldsymbol{E}^\pm$ is a c-number and in the latter case an operator. The optical matrix elements for the vacuum-to-exciton and exciton-to-biexciton transitions $\boldsymbol{P}_{0x}(\boldsymbol{r})$ and $\boldsymbol{P}_{xb}(\boldsymbol{r})$, respectively, can be computed according to [14,15]

$$\begin{aligned} \boldsymbol{P}_{0x}(\boldsymbol{r}) &= \boldsymbol{\mu}\, \Psi_x(\boldsymbol{r},\boldsymbol{r}), \\ \boldsymbol{P}_{xb}(\boldsymbol{r}) &= \boldsymbol{\mu} \int d\boldsymbol{r}_e d\boldsymbol{r}_h\, \Psi_x^*(\boldsymbol{r}_e,\boldsymbol{r}_h) \Psi_b(\boldsymbol{r},\boldsymbol{r},\boldsymbol{r}_e,\boldsymbol{r}_h) , \end{aligned} \tag{7}$$

where Ψ_x and Ψ_b are the exciton and biexciton wavefunctions, respectively. Here we have accounted for the fact that the photo-generated electron and hole are created at the same position $\boldsymbol{r}$, and in $\boldsymbol{P}_{xb}(\boldsymbol{r})$ the positions of the additional electron and hole remain at the same position $\boldsymbol{r}_e$ and $\boldsymbol{r}_h$. For the excitation of the nanostructure through the optical fiber tip, fig. 1(a), the electric field can be described as classical. The Rabi energies $\Omega(\boldsymbol{r}_{\rm tip})$, which describe the interaction between the nearfield excitation and the quantum dot, become a convolution of the dipole elements (7) with the electromagnetic profile $\boldsymbol{E}_\omega(\boldsymbol{r}_{\rm tip} - \boldsymbol{r})$ of the nearfield tip [see eq. (5)]. Throughout we assume a cw excitation with a single frequency ω. The coherent time evolution is then given by the master equation [15,17]

$$\dot{\boldsymbol{\rho}} = -i \left[\boldsymbol{\Delta} + \boldsymbol{\Omega} + \boldsymbol{\Omega}^\dagger, \boldsymbol{\rho} \right] , \tag{8}$$

with $\boldsymbol{\rho}$ be the density matrix of quantum dot states, $\boldsymbol{\Omega}$ the matrix of the tip-dependent Rabi energies, and $\boldsymbol{\Delta}$ the detunings of the exciton and biexciton energies from the driving frequency, i.e. $\Delta_x = E_x - \omega$ and $\Delta_b = E_b - 2\omega$. Through the external nearfield excitation electron-hole states are created which decay by emission of photons. To account for such emissions we have to adopt an open-system description [18], where the nearfield excitation introduces two conceptual problems: first, the presence of the optical fiber may lead to a modification of the dielectric environment which, in turn, may influence the photon modes and couplings. Secondly, through the Rabi energies $\boldsymbol{\Omega}$ in eq. (8) the exciton and biexciton states become mixed. Scattering thus occurs between renormalized states, that result from the interplay of the coherent excitation with the incoherent photon scatterings themselves. In other words, exciton and biexciton states cannot be decoupled from the light fields, and the whole system has to be treated self-consistently. A convenient approach to account for such renormalization effects is to describe photon emission processes within lowest order time-dependent perturbation theory [18,15]

$$\dot{\rho}(t) \cong - \int_{t_0}^{t} dt'\, {\rm tr}_R \left[V(t), \left[V(t'), \rho_R \otimes \rho(t) \right] \right] , \tag{9}$$

with $V(t)$ the light-matter coupling (6) for quantized field operators $\boldsymbol{E}^\pm$ in the interaction representation, ρ_R the photon denstity operator, assumed to represent the photon vacuum, and ${\rm tr}_R$ denoting the trace over the photon degrees of freedom. After performing in eq. (9) such trace, the whole effect of the photon environment on the quantum dot states is embodied in the correlation functions $\langle E_i^+(\boldsymbol{r},t) E_j^-(\boldsymbol{r}',t') \rangle$, with i and j labeling the three spatial directions. To compute these correlation functions we fortunately do not have to introduce a proper quantization of photon modes, which would be particularly cumbersome for absorbing media. Rather we can make use of the fluctuation-dissipation theorem [19,20]

$$\left\langle 0 \middle| E_i^+(\boldsymbol{r},\omega) E_j^-(\boldsymbol{r}',\omega) \middle| 0 \right\rangle = 4k^2\, \Im m\, G_{ij}(\boldsymbol{r},\boldsymbol{r}';\omega) \tag{10}$$

that relates the vacuum correlation functions for the electric field components to the conventional Green tensor G_{ij} of Maxwell's theory [21]. Here we have introduced a Fourier transform in time. Upon insertion of the Green tensor into the master equation (9) the resulting time integral then accounts for the temporal buildup of scatterings. Owing to the destructive interference of different photon modes the time period over

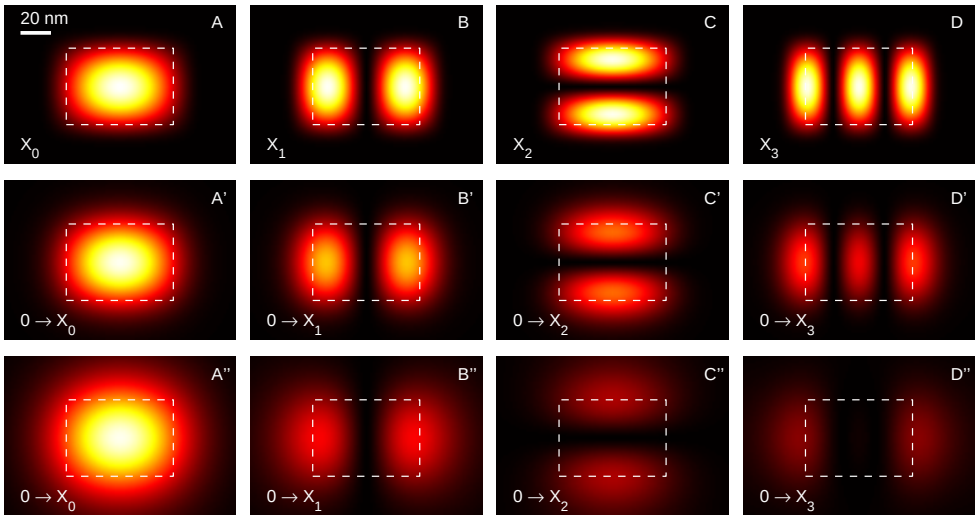

Fig. 2. (a–d) Real-space map of the square modulus of the wavefunctions for the exciton (a) ground state, (b) first, (c) second, and (d) third excited state. The dashed lines indicate the boundaries of the assumed interface fluctuation. (a'–d') Near-field spectra for a spatial resolution of 25 nm and (a"–d") 50 nm. With the material parameters of Ref. [13] we find energies of −8.686, −8.442, −8.128, and −8.043 meV for the exciton groundstate and the first three excited exciton states, respectively, and −17.264 meV for the biexciton groundstate; exciton (biexciton) energy zero is given by the energy of the two-dimensional exciton (biexciton) of the narrow quantum well [14].

which the integral has to be extended into the past will be rather short. A rough estimate is provided by Heisenberg's energy-time uncertainty principle, which for a typical energy of 1 eV exchanged in a photon scattering gives a time period $\delta t \sim \hbar/\delta E \sim 1$ fs. This time scale is much shorter than the pico to nano second timescale of photo excitation and photon decay. We thus compute the Green functions $G_{ij}(\boldsymbol{r}, \boldsymbol{r}'; \omega_0)$ at a frequency ω_0 of the bandgap and ignore the time integration in the master equaltion (9) by setting $t' = t$. This so-called white-noise approximation is a standard procedure in quantum optics [18], and can be backed by a more rigorous analysis [15]. In the follwoing we assume for simplicity that the radiative decay of excitons and biexcitons is not drastically altered by the presence of the SNOM tip and replace the Green tensor by the free one, i.e. $\Im m\, G_{ij}(\boldsymbol{r}, \boldsymbol{r}'; \omega_0) \cong \delta_{ij}\, \omega_0/6\pi c$. This is a reasonable assumption since the photons can be emitted into any solid-angle direction. The time evolution of the system under consideration is then described by the master equation [15]

$$\dot{\boldsymbol{\rho}} = -i \left[\boldsymbol{\Delta} + \boldsymbol{\Omega} + \boldsymbol{\Omega}^\dagger, \boldsymbol{\rho}\right] - \frac{\Gamma_0}{2}\left(\boldsymbol{M}\boldsymbol{M}^\dagger\boldsymbol{\rho} + \boldsymbol{\rho}\boldsymbol{M}\boldsymbol{M}^\dagger - 2\boldsymbol{M}^\dagger\boldsymbol{\rho}\boldsymbol{M}\right) + \boldsymbol{\Gamma}_{\rm ph}(\boldsymbol{\rho})\,, \tag{11}$$

with Γ_0 the usual Wigner-Weisskopf decay rate, M_{0x} and M_{xb} the optical far-field matrix elements, which are obtained by integrating the elements (7) over the entire space [17], and $\boldsymbol{\Gamma}_{\rm ph}$ accounting for additional phonon scatterings [22] described in Lindblad form. The steady-state solutions, which results from the interplay of excitation and relaxation, and the luminescence spectra are finally obtained from Eq. (11) by computing the eigenvalues and eigenvectors of the Liouvillian and making use of the quantum regression theorem [18].

3. Results

In the first row of fig. 2 we show the real-space maps of the square modulus of the exciton (a) ground and (b–d) excited states. The computed excitonic states exhibit symmetries reminiscent of the two-dimensional box-like confinement, i.e., an s-like exciton groundstate (fig. 2a), two p-like excited states of lowest energy with nodes along x (fig. 2b) and y (fig. 2c), and two nodes along x for the third excited exciton state (fig. 2d). Finally, the biexciton groundstate B_0 (inset of fig. 1b)

shows a stronger degree of localization than the exciton groundstate X_0, which we attribute to the larger extension of the biexciton complex owing to the weaker biexciton binding [11,14,23]. In the second and third rows of fig. 2 we report our calculated optical near-field spectra for spatial resolutions of approximately 25 and 50 nm. It should be noted that the first (fig. 2b) and second excited state (fig. 2c) are dipole forbidden, but have large oscillator strengths for both resolutions. Note also that, as a result of interference effects, the spatial maps at finite spatial resolutions differ somewhat from the wavefunction maps, particularly for the excited states: the apparent localization is weaker and, in (d), the central lobe is very weak for both resolutions.

In the following we investigate whether dark quantum dot states can be directly probed in SNOM. For convenience we consider a two-photon excitation of biexcitons, fig. 1(b), where, because of the biexciton binding energy $\delta E_b \sim 4$ meV [24], the luminescence from the $B \to X$ and $X \to 0$ recombinations is red- and blue-shifted, respectively, and can thus be spectrally discriminated. We assume that the heterostructure is excited through a strongly inhomogeneous field emitted by a fiber tip at the two different spots A and B shown in Fig. 1(b). We also assume that the luminescence is detected somewhere in the far-field but not necessarily through the SNOM tip. Figure 3 shows the corresponding luminescence spectra. For tip position A (center of the dot) the field does not break the symmetry of the underlying quantum states. Accordingly, only the ground state biexciton B_0 can be excited, whereas the transition to B_1 is forbidden because of symmetry, as in the far-field case. Correspondingly the luminescence spectra consist of two equally strong peaks associated to the $B_0 \to X_0$ and $X_0 \to 0$ transitions. The line broadenings are due to photon emissions and are as large as $\Gamma \sim 100$ μeV for the large coherence volumes of the exciton and biexciton states. Note that the far-field luminescence spectrum (not shown here) is almost identical to that of fig. 3(a).

When the dot is excited at tip position B, which does not coincide with the symmetry center of the heterostructure, an additional ultra-narrow peak appears, indicated with B_1 in Fig. 3(b), which is due to the excitation of the biexciton B_1. Because this dark state couples weakly to photons, its lifetime is orders of magnitude larger than that of the bright B_0 state.

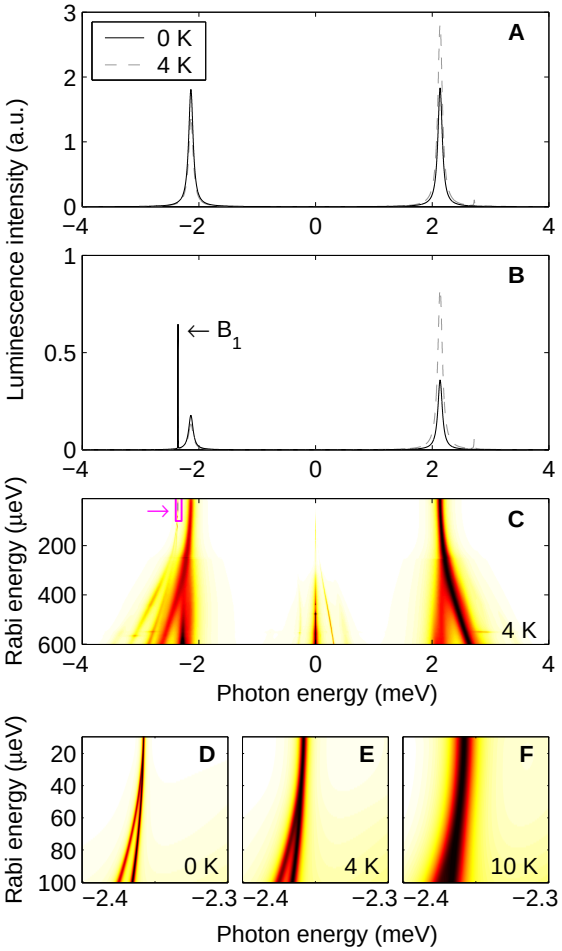

Fig. 3. Near-field luminescence spectra for two selected tip positions A and B, as indicated in Fig. 1(b), and different temperatures. At position A the usual far-field selection rules apply, and the spectrum consists of two peaks associated to the $B_0 \to X_0$ and $X_0 \to 0$ transitions. At position B an additional ultra-narrow peak appears, which is due to the radiative decay of the dark biexciton state B_1. Panel C shows the power dependence of the optical spectra at tip position B which have been normalized with respect to the respective maxima. The power and temperature dependence of the dark-state transition B_1 is magnified in panels D, E, and F. Photon energy zero is given by ω.

At the lowest excitation powers the broadening of this additional peak is dominated by phonon scattering ($\Gamma \sim 1$ μeV for zero temperature). However, its appearence in the luminescence spectrum indicates a substantial excitation-induced mixing of excitonic states. With increasing excitation power this mixing becomes

stronger, resulting in a further peak broadening and the appearence of new emission lines as shown in panel c. In the following we concentrate on the low power regime, corresponding to the spectra shown in Figs. 3(a) and (b), where the dominant mixing is between the bright B_0 and dark B_1 biexciton state, whereas exciton states become less mixed because of the off-resonant excitation and the larger level splittings due to the lighter exciton mass [14]. The power and temperature dependence of the dark-state transition B_1 is magnified in panels (d) to (f) We observe an ac-Stark effect and a splitting of the line at relatively small Rabi energies Ω. Similarly to the Mollow spectrum of a driven two-level system [18], this splitting is due to a strong light-biexciton coupling and occurs when the line broadening Γ becomes comparable to the effective Rabi frequency (note that the B_1 transition is excited non-resonantly). With increasing temperature Γ increases and the Rabi splitting occurs at higher field strengths Ω [Figs. 3(e) and (f)]. The essentials of these findings are expected to prevail for dot confinements with lower symmetry [17].

4. Conclusions

In conclusion, we have studied scanning nearfield optical microscopy of semiconductor nanostructures. A general theoretical framework has been developed that accounts on the same footing for the quantum dot carrier states, the excitation of the nearfield probe, the optical decay of the carrier states in presence of a possibly modified dielectric environment, and for other environment couplings. When the quantum dot is excited through the SNOM tip (illumination mode) the far-field selection rules are broken and it becomes possible to excite dark excitonic states, weakly coupled to the light, which show up as additional ultra-narrow peaks in the luminescence spectra. In the future, similar wavefunction mapping is expected to become possible for other scanning probe techniques, such as optical nano antennas [25], which might pave the way for optical nano imaging of molecules or biological structures.

Acknowledgements

I am indebted to Guido Goldoni and Elisa Molinari for generous support and most helpful discussions. Work supported in part by the EU under the TMR network "Exciting" and the Austrian science fund FWF under project P15752–N08.

References

[1] J. B. Pendry, Phys. Rev. Lett. 85 (2000) 3966.

[2] M. A. Paesler and P. J. Moyer, *Near-Field Optics: Theory, Instrumentation, and Applications* (Wiley, New York, 1996).

[3] B. Hecht, B. Sick, U. P. Wild, V. Deckert, R. Zenobi, O. J. F. Martin, and D. W. Pohl, J. Chem. Phys. 112 (2000) 7761.

[4] E. Betzig, J. K. Trautman, T. D. Harris, J. S. Weiner, and R. L. Kostelak, Science 251 (1991) 1468.

[5] H. F. Hess, E. Betzig, T. D. Harris, L. N. Pfeiffer, and K. W. West, Science 264 (1994) 1740.

[6] J. R. Guest, T. H. Stievater, Gang Chen, E. A. Tabak, B. G. Orr, D. G. Steel, D. Gammon, and D. S. Katzer, Science 293 (2001) 2224.

[7] W. E. Moerner, T. Plakhotnik, T. Irngartinger, U. P. Wild, D. W. Pohl, and B. Hecht, Phys. Rev. Lett. 73 (1994) 2764.

[8] C. Hettich, C. Schmitt, J. Zitzmann, S. Kühn, I. Gerhardt, and V. Sandoghdar, Science 298 (2002) 385.

[9] C. Chicanne, T. David, R. Quidant, J. C. Weber, Y. Lacroute, E. Bourillot, A. Dereux, C. Golas de Francs, and C. Girard, Phys. Rev. Lett. 88 (2002) 097402.

[10] C. Ropers, D. J. Park, G. Stibenz, G. Steinmeyer, J. Kim, D. S. Kim, and C. Lienau, Phys. Rev. Lett. 94 (2005) 113901.

[11] K. Matsuda, T. Saiki, S. Nomura, M. Mihara, Y. Aoyagi, S. Nair, and T. Takagahara, Phys. Rev. Lett. 91 (2003) 177401.

[12] O. Mauritz, G. Goldoni, F. Rossi, and E. Molinari, Phys. Rev. Lett. 82 (1999) 847.

[13] C. Simserides, U. Hohenester, G. Goldoni, and E. Molinari, Phys. Rev. B 62 (2000) 13657.

[14] U. Hohenester, G. Goldoni, and E. Molinari, Appl. Phys. Lett. 84 (2004) 3963.

[15] U. Hohenester, Eds. M. Rieth and W. Schommers, *Handbook of Theoretical and Computational Nanotechnology* (American Scientific Publishers, Stevenson Ranch, CA, 2006).

[16] R. Zimmermann, F. Große, and E. Runge, Pure and Appl. Chem. 69 (1997) 1179.

[17] U. Hohenester, G. Goldoni, and E. Molinari, Phys. Rev. Lett. 95 (2005) 195429.

[18] D. F. Walls and G. J. Millburn, *Quantum Optics* (Springer, Berlin, 1995).

[19] C. H. Henry and R. F. Kazarinov, Rev. Mod. Phys. 68 (1996) 801.

[20] S. Scheel, J. K. Pachos, E. A. Hinds, and P. L. Knight; in W. Pötz, J. Fabian, and U. Hohenester, editors, *Quantum Coherence in Matter*, Lecture Notes in Physics 689 (Springer, Berlin, 2006).

[21] C. Girard, Rep. Prog. Phys. 68 (2005) 1883.

[22] U. Bockelmann, Phys. Rev. B 48 (1993) 17637.

[23] E. Runge and C. Lienau, Phys. Rev. B 71 (2005) 035347.

[24] A. Zrenner, L. V. Butov, M. Hagn, G. Abstreiter, G. Böhm, and G. Weimann, Phys. Rev. Lett. 72 (1994) 3382.

[25] J. N. Farahani, D. W. Pohl, H. J. Eisler, and B. Hecht, Phys. Rev. Lett. 95 (2005) 017402.